Anti-tyrosinase and antioxidant activity of meroterpene bakuchiol from Psoralea corylifolia (L.)

A. Cariola, M. El Chami, J. Granatieri, L. Valgimigli. **Anti-Tyrosinase and Antioxidant Activity of Meroterpene Bakuchiol from *Psoralea corylifolia* (L.).**

Food Chemistry, **2023**, *405*, 134953

Anti-Tyrosinase and Antioxidant Activity of Meroterpene Bakuchiol from *Psoralea corylifolia* (L.)

Alice Cariola,[a,b] Madeleine El Chami,[a] Jonathan Granatieri,[a] and Luca Valgimigli,[a,b,*]

[a] University of Bologna, Department of Chemistry "G. Ciamician", Via S. Giacomo 11, 40126 Bologna, Italy

[b] Tecnopolo di Rimini, Via Dario Campana 71, 47922, Rimini, Italy

* to whom correspondence should be addressed. E-mail: luca.valgimigli@unibo.it; Tel. +390512095683

Abstract

Bakuchiol is gaining major interest for treatments against skin photoaging. The kinetics of mushroom tyrosinase inhibition by bakuchiol, by real-time oxygen sensing and UV-Vis monitoring (475nm), showed competitive inhibition with average K_i constant (μM, 30°C, pH 6.8) of 6.71±1.23 and 1.15±0.34 for monophenolase and diphenolase reactions respectively, with respective IC_{50} 37.22±5.18 and 6.91±0.96 ~ at 1 mM substrate, compared to kojic acid IC_{50} 34.02±5.51 and 16.86±3.28 μM. Fluorescence quenching showed a single binding mode with formation constant K_a 1.02×10^6 M^{-1}. The antioxidant activity was studied by inhibited autoxidation of styrene and cumene (PhCl, 30°C) affording inhibition constant k_{inh}=18.1±6.6 ($10^4M^{-1}s^{-1}$, 30°C) and of MeLin in Triton™ X-100 micelles giving k_{inh}=0.16±0.03 ($10^4M^{-1}s^{-1}$, 37°C). Stoichiometric factor was 1.9±0.1. ReqEPR spectroscopy afforded the BDE(OH) as 81.7±0.1 kcal/mol. Bakuchiol is a potent tyrosinase inhibitor with good antioxidant activity having major potential as natural food preservative against oxidation and food-browning.

Keywords: bakuchiol; skin-whitening; melanin; food browning; antioxidant; peroxyl radicals.

Compounds investigated in this study:

(*S*)-Bakuchiol, CAS 10309-37-2 (PubChem CID: 5468522)

O-methylbakuchiol, CAS 10309-44-1 (PubChem CID: 14610678)

Kojic acid, CAS: 501-30-4 (PubChem CID: 3840)

Mushroom Tyrosinase (EC 1.14.18.1), CAS: 9002-10-2

1. Introduction

Psoralea corylifolia (L.) is an annual erect herb (30-180 cm in height) native of India and the subtropical regions, which has wide and long-standing use in Traditional Chinese Medicine and in Indian Ayurvedic medicine (Chopra, Dhingra & Dhar, 2013; Alam, Khan & Asad, 2018). The edible seeds (legumes) have the highest medicinal value for the content in bioactive phytochemicals including sterols, flavonoids, chalcones, psoralenes, terpenes and, most notably, the meroterpene bakuchiol (Figure 1) (Chopra et al., 2013), named after the Indian traditional name of the plant (bakuchi, or baguchi, or babchi).

Several studies have outlined important and diverse bioactivities of bakuchiol, such as antinflammatory, antimicrobial, anticancer, estrogenic, protection from organ damage, from diabetes and from anxiety and neurological disorders (Chopra et al., 2013; Alam et al., 2018; Oh et al., 2010). However, the main interest in recent research has been polarized by the structural similarity with retinol (Vitamin A), which enables mimic bioactivity, particularly in dermatological applications (Krishna, Edachery & Athalathil, 2022), such as in anti-acne, anti-psoriasis and anti-age treatments (Chaudhuri & Bojanowski, 2014). Clinical investigations proved similar efficacy to retinol in topical skincare treatments against photoaging, accompanied by much lower side effects (Dhaliwal et al., 2019).

Such efficacy is in part attributed to a reported antioxidant activity (Dhaliwal et al., 2019; Haraguchi, Inoue, Tamura & Mizutani, 2000). The reactivity of bakuchiol with selected radicals was investigated and its ability to protect rat brain homogenates from autoxidation was shown using the TBARS assay (Adhikari et al., 2003); however, the absolute antioxidant activity and the trapping of most relevant alkylperoxyl radicals, which represent the main mechanism sustaining direct antioxidant activity was not determined, allowing no quantitative comparison with other antioxidants and no rational exploitation of its properties.

Interestingly, clinical investigation also outlined a skin depigmenting activity, which was judged not due to the most common mechanism, *i.e.* the inhibition of tyrosinase enzyme activity (West, Alabi &

79 Deng, 2021). Other studies attributed the skin depigmenting activity to reduction of pre-formed
80 melanin (owing to the antioxidant activity), or to the blocking of α-melanocyte-stimulating hormone
81 activation, as well as to (not investigated) inhibition of tyrosinase (Dhaliwal et al., 2019). Inhibition
82 of tyrosinase was shown using immobilized mushroom tyrosinase (mTYR) with an electrophoresis
83 assay and it was also supported by molecular docking (Cheng & Chen, 2017); however, the reported
84 IC_{50} value of 100.30 μM for inhibition of diphenolase activity, much higher than for reference
85 inhibitor kojic acid (5.55 μM) (Cheng & Chen, 2017), appears too high to justify the depigmenting
86 efficacy outlined in clinical studies, leaving the matter essentially unsettled. Moreover, the inhibition
87 mechanism and the Michaelis-Menten related constants, which are most relevant in quantifying
88 enzyme inhibition, have never been determined.
89 Owing to the major importance of bakuchiol as emerging bioactive food component (Chopra et al.,
90 2013; Alam et al. 2018; Chaudhuri & Bojanowski, 2014; Dhaliwal et al., 2019; West et al., 2021),
91 and to the current high interest in plant-derived depigmenting compounds (Mahdavi,
92 Mohammadsadeghi, Mohammadi, Saadati & Nikfard, 2022; Zhu et al., 2022; He, Fan, Liu, Li &
93 Wang, 2021; Yang et al., 2021; Song, et al., 2021; Panzella & Napolitano, 2019), particularly for their
94 efficacy in post-harvest food protection (Zhou et al., 2022), we set up to fill in such gap of knowledge.
95 The kinetics of mTYR inhibition was investigated in depth, by exploiting our newly developed and
96 validated method based on real-time oxygen sensing during tyrosinase reaction (Guo, Cariola, Matera,
97 Gabbanini & Valgimigli, 2022), which we matched to the conventional spectrophotometric and
98 spectrofluorometric approaches for enhanced reliability. Additionally, we investigated the
99 antioxidant activity of bakuchiol by state-of-the-art inhibited autoxidation studies both in
100 homogenous solution and in heterogeneous system (Amorati & Valgimigli, 2018; Guo, Baschieri,
101 Amorati & Valgimigli, 2021; Guo et al., 2021b), and by electron paramagnetic resonance (EPR)
102 (Amorati, Pedulli, Valgimigli, Johansson & Engman, 2010), so to complete the picture, affording the
103 mechanism and absolute kinetics and thermodynamics of peroxyl radical trapping (Valgimigli & Pratt,
104 2015).

Our hypothesis was that bakuchiol's anti-tyrosinase potency is substantially higher that previously suggested and that the mechanism of its antioxidant activity would require significant revision. Our hypothesis was particularly that bakuchiol has a previously unrecognized great potential as natural food preservative, which stems from the combined abilities to protect from air oxidation and from enzymatic food browning.

2. Materials and Methods

2.1 Materials

(*S*)-(+)-Bakuchiol (4-[(3*S*,1*E*)-3-ethenyl-3,7-dimethylocta-1,6-dien-1-yl]phenol; 99%) was from Cymit Quimica (Barcellona, Spain). L-Tyrosine (⩾ 98%), L-DOPA (3,4-dihydroxy-L-phenylalanine; ⩾ 98%), kojic acid (5-hydroxy-2-hydroxymethyl-4H-4-pyranone; ⩾ 98.5%) and mushroom tyrosinase (mTYR; EC 1.14.18.1, activity = 3130 units/mg) were purchased from Sigma-Aldrich and used without further purification. Fresh mTYR solutions were prepared every day and tyrosinase activity was analysed spectrophotometrically to adjust solutions to fixed tyrosinase Sigma units for consistent results. Briefly, one Sigma unit corresponds to the amount that will cause an increase in absorbance at 280 nm of 0.001 per minute at pH 6.8 in a 3 mL reaction mixture containing L-tyrosine. Sigma units were used throughout this study. One Sigma unit corresponds to 1.65×10^{-4} international units (I.U.) for monophenolase activity and to 2.24×10^{-2} I.U. for diphenolase activity, as defined by Fenoll et al. (2002). AAPH (2,2'-azobis(2-methylpropionamidine) dihydrochloride), methyl linoleate (⩾ 98%) and Triton™ X-100, were used as received. AIBN (2,2′-Azobis(isobutyronitrile); 98%) was recrystallized from methanol, while 2,4,6-tri-*tert*-butylphenol (TBP, 98%) was recrystallized from hexane. Stock solutions of AAPH or AIBN in the desired solvents were prepared immediately prior to use and/or maintained for maximum 2h or 4h, respectively, at 4°C between subsequent uses, to avoid significant decomposition. Cumene (98%) and styrene (⩾ 99%) were purified by double percolation through silica and activated basic alumina columns. Solvents and other chemicals were

of the highest grade commercially available (Sigma-Aldrich, Merck, VWR; Milan, Italy) and were used as received.

2.2 Synthesis of (S)-(+)-Bakuchiol methyl ether

MeOBak ((3*S*,1*E*)-1-(3,7-dimethyl-3-vinylocta-1,6-dien-1-yl)-4-methoxybenzene) was prepared by cautious addition of 0.2 mmol of bakuchiol (in dry DMF) to a suspension of 1.4 eq. NaH in dry DMF at 0°C under N_2. The mixture was stirred for 30 min while allowing to reach r.t., then MeI (1.4 eq) was added dropwise and the mixture was stirred for 4h at r.t. then quenched with brine and extracted with hexane. The dried (Na_2SO_4) extract was evaporated under vacuum do afford a yellowish oil which was purified by column chromatography on silica gel, eluting with hexane/EtOAc 95:5 (yield 85%; purity 99% by GC-MS, see Appendix).

^{1}H NMR (400 MHz; $CDCl_3$) δ 7.30 (2H, d, *J* = 9 Hz), 6.80 (2H, d, *J* = 9 Hz,), 6.30 (1H, d, *J* = 16 Hz), 6.10 (1H, d, *J* = 16 Hz), 5.88 (1H, dd, *J* = 18, 11 Hz), 5.11 (1H, t, *J* = 7 Hz), 5.02 (2H, m), 3.80 (3H, s, OC<u>H</u>$_3$), 1.95 (2H, dt, *J* = 9, 8 Hz), 1.70 (3H, s), 1.57 (3H, s), 1.50 (2H, m), 1.20 (3H, s) ppm; in agreement with literature (Hu & Brenner-Moyer, 2022).

MS (EI$^+$, 70 eV) *m/z*: 271 (2), 270 (M$^+$, 10), 255 (3), 227 (10), 188 (17), 187 (100), 173 (10), 172 (23), 159 (29), 158 (18), 144 (19), 135 (19), 121 (66), 93 (24), 91 (18), 83 (17), 79 (25), 69 (29), 55 (39), 41 (69).

2.3 mTYR kinetic studies by UV-vis spectrophotometry

Kinetic evaluation of tyrosinase reaction with or without inhibitor was carried out using UV-Vis spectrophotometry similarly to previous methods (Copeland, 2000; Song et al., 2021; Yu & Fan, 2021), following our recent protocol (Guo et al., 2022). Measurements were performed at 30°C in phosphate buffer (50 mM, pH 6.8) in polystyrene low-volume cuvettes (1.5 mL, *l* = 1 cm) with a double-beam spectrophotometer. L-Tyrosine and L-Dopa (5 levels, 0.125-2 mM) were used as the substrate of mushroom tyrosinase (mTYR, 0.5-5.0 U/ml) for monophenolase and diphenolase reactions, respectively. Bakuchiol (0 to 12 μM) and kojic acid (0 to 50 μM) were comparatively tested as inhibitors. Absorbance of dopachrome was measured at 475 nm for a time-period of 20 to 60 min

reading the solution against a reference cuvette containing all reaction components except the substrate. Absorbance variation *vs* time at different substrate concentration allowed to obtain initial velocity (V = ΔA/Δmin) which was converted in μM/min according to Lambert-Beer law as follows: V (μM/min) = V (ΔA/Δmin) × 10^6 / $\varepsilon_{\lambda max}$× *l*. The molar extinction coefficient (ε) for dopachrome at λ_{max}= 475 nm is 3700 M^{-1} cm^{-1}. Michaelis-Menten parameters (K_m e V_{max}) were obtained by processing initial velocity *vs* substrate concentration data by nonlinear fitting to M-M equation (1), using Sigmaplot 11.0 (Systat Software Inc., San Jose, California) (Guo et al., 2022). Linearized Lineweaver-Burk equation (2) was used to identify the inhibition mode (Copeland, 2000). In both equations, *V* indicates the measured initial rate of reaction, [*S*] is the initial substrate concentration, while V_{max} and K_m are respectively the maximum reaction rate (at saturating substrate concentration) and the M-M constant. (the substrate concentration yielding half-maximum reaction rate).†

$$V = \frac{V_{max}\,[S]}{K_m + [S]} \quad (1)$$

$$\frac{1}{V} = \frac{K_m}{V_{max}\,[S]} + \frac{1}{V_{max}} \quad (2)$$

2.4 mTYR kinetic studies by oximetry

Evaluation of tyrosinase monophenolase and diphenolase kinetics and inhibition by bakuchiol or kojic acid was carried out by monitoring the oxygen consumption, at 30°C, by miniaturized oxygen sensing apparatus, based on NIR (760-790 nm) fluorescence quenching, which has previously been described in detail (Guo et al., 2022). The samples were contained in stirred 2.4 mL glass flasks, immersed in a water bath. The oxygen consumption was recorded every second, and all reaction components were maintained as those set for UV-vis spectrophotometry. The raw data collected directly from the oxygen sensor is a percentage (P) of the saturating oxygen concentration in the sample, corresponding to 0.236 mM at 30°C which reflects in the sensor reading as 20% (P_0). Thus, the oxygen concentration during the enzymatic oxidation of L-DOPA or L-tyrosine were converted into mM by the equation: [O_2] (mM) = P × 0.236 (mM) / 20%. The initial rate of oxygen consumption was obtained as (ΔP) *vs* time (in seconds) by regression of the initial data range of oxygen

consumption, and it was converted by equation: V (μM/min) = V ($\Delta P/\Delta t$) × 0.236 × 10^3 × 60 / P_0 which was used for analysis by non-linear fitting to Michaelis-Menten kinetics (eq. 1). Previous studies indicate that the stoichiometry of O_2 uptake / dopachrome formation is 1.5:1 and 1:1 for substrate L-tyrosine and L-DOPA, respectively (Guo et al. 2022), therefore the rate of O_2 uptake recorded for monophenolase reaction was divided by 1.5.[†]

2.5 Fluorescence quenching studies

Fluorescence spectra arising from interactions between bakuchiol and tyrosinase were recorded by a fluorescence spectrometer (Horiba FluroMax-4) at r.t. similarly to literature (Yu & Fan, 2021). A 2.5 mL solution of tyrosinase (20 U/mL) in 50 mM sodium phosphate buffer (pH 6.8) was placed in quartz cuvettes and a bakuchiol stock solution in methanol was added portionwise, for a total of 10 additions, to obtain various concentration of bakuchiol in the solution, from 0 to 1.320 μM. Each resultant solution was incubated for 1 min to equilibrate, before measurement. The excitation wavelength was set at 280 nm and the emission spectra were collected from 290 to 500 nm with excitation and emission slits kept at 5 nm.

2.6 Autoxidation studies in homogenous solution

Autoxidation experiments were performed in a two-channel oxygen uptake apparatus, based on a Validyne DP 15 differential pressure transducer built in our laboratory (Amorati, Pedulli & Valgimigli, 2011; Baschieri, et al., 2019; Amorati et al., 2016). In a typical experiment, an air-saturated solution of the oxidizable substrate containing AIBN (0.01-0.1M) was equilibrated at 30 °C with an identical reference solution containing excess 2,2,5,7,8-pentamethyl-6-hydroxychromane (PMHC, 25 mM). After equilibration, and when a constant O_2 consumption was reached, a stock solution of the antioxidant (typically 1.0 mM in PhCl) was injected in the sample flask, so to reach the desired concentration in the range 1-20 μM in the sample flask. The oxygen consumption in the sample was measured after calibration of the apparatus from the differential pressure recorded with time between the two channels. Initiation rates, R_i, were determined for each condition in preliminary

experiments by the inhibitor method (eq. 3), where τ is the length of the inhibition period, using TOH as a reference antioxidant (Guo et al., 2021a; Guo et al., 2021b).

The inhibition rate constant for peroxyl radical trapping k_{inh} was obtained from oxygen consumption plots by eqs. 4 or 5, where k_p, and $2k_t$, are the rate constants for chain propagation and termination of the substrate, R_0 and R_{inh} are respectively the rate of oxygen consumption ($-d[O_2]/dt$) in the absence and presence of the antioxidant, while n is the stoichiometric factor, *i.e.* the number of peroxyl radicals trapped by one molecule of antioxidant (Amorati & Valgimigli, 2018; Amorati et al., 2016). Styrene (k_p = 41 $M^{-1}s^{-1}$; $2k_t = 4.2\times10^7$ $M^{-1}s^{-1}$, at 30°C) and cumene (k_p = 0.34 $M^{-1}s^{-1}$; $2k_t = 4.5\times10^4$ $M^{-1}s^{-1}$, at 30°C) were used as the oxidizable substrates (Amorati et al., 2011; Baschieri et al., 2019).

$$\tau = \frac{n[Antiox.]}{R_i} \quad (3)$$

$$-\frac{d[O_2]}{dt} = \frac{k_p[Substrate]R_i}{nk_{inh}[Antiox]} \quad (4)$$

$$\frac{R_0}{R_{inh}} - \frac{R_{inh}}{R_0} = \frac{nk_{inh}[Antiox]}{\sqrt{2k_tR_i}} \quad (5)$$

2.7 Autoxidation studies in aqueous micelles

Measurement were performed as previously described (Konopko & Litwinienko, 2022), with modifications. In a typical experiment, 2.5 mL of air-saturated buffered (PBS, 50 mM, pH 7.4) aqueous dispersion of MeLin (final concentration 2.74 mM) in Triton™ X-100 (final concentration 8 mM) micelles were prepared by vortex mixing, then adding a freshly prepared stock solution of AAPH (final concentration 5 mM), immediately followed by addition 4-16 μL of a (0.5-1 mM) stock solution of the antioxidant in acetonitrile (final concentration of 2-8 μM) at room temperature. After brief additional vortex stirring (5-10 sec.) the mixture used to fill in a sealed 2.4 mL glass vial provided with a PTFE-coated stirring bar. The sample was equilibrated at 37 °C in a thermostatted bath equipped with a sealed magnetic stirrer and O_2 consumption was recorded. Oxygen concentration was monitored with the same equipment described for mTYR kinetics and data were similarly treated by the equation: V (M/s) = V ($\Delta P/\Delta t$) × 0.210 × 10^{-3} / P_0, where P_0 is the initial 20%

O_2 saturation reading that corresponds to 0.210 mM at 37°C. Oxygen consumption in the presence of the antioxidant was compared with that recorded with identical reference mixtures lacking the antioxidant. The inhibition rate constant was obtained from oxygen consumption plots by eqs. 3-5, as described for autoxidation studies in homogenous solution, using k_p = 36 $M^{-1}s^{-1}$ for MeLin in micelles (Konopko & Litwinienko, 2022).

2.8 EPR measurements

Deoxygenated *tert*-butylbenzene solutions containing the phenols (0.01-0.001 M) and di-*tert*-butyl peroxide (10% v/v) were sealed under nitrogen in a suprasil quartz EPR tube. The sample was inserted in the thermostatted (30°C) cavity of an X-band EPR spectrometer and photolyzed with a mercury-xenon lamp (240-400 nm, max 4500 mW/cm^2). Spectra were recorded with the following settings: modulation amplitude 0.1-1 Gauss, sweep width 60 Gauss, modulation frequency 100 kHz, frequency 9.76 GHz, sweep time 60s, microwave power 0.1-1 mW. Measured *g*-factors, were corrected with respect to that of the perylene radical cation in concentrated H_2SO_4 (g = 2.00258) (Amorati et al., 2011; Valgimigli et al., 2000). When using mixtures of TBP and bakuchiol in ReqEPR experiments, the molar ratio of the two equilibrating radicals was obtained from the EPR spectra and used to determine the equilibrium constant, K_{eq} (Johansson et al. 2010; McGrath, Garrett, Valgimigli & Pratt, 2010). Different irradiation power levels (20% to 100%) and different ratios of the two phenols were tested to guarantee that the two species where at the equilibrium (Amorati et al., 2010). Spectral parameters and relative radical concentrations were determined by comparison of the digitized experimental spectra with computer simulated ones, as previously described (Amorati et al., 2010; Amorati et al., 2011; Brigati, Lucarini, Mugnaini, & Pedulli, 2002).

2.9 Statistical analysis

Each measurement was performed at least in triplicate. Values of V_{max} and V_{max}^{app}, and of K_m and K_m^{app} in the absence and presence of inhibitors were determined from non-linear regression of M-M plots based on 5-6 concentrations of the substrate, which were analysed by Shapiro-Wilk Test with significance set at $P \leq 0.05$. Results are expressed as regression value ± standard error.

3. Results

3.1 Kinetics of mTYR inhibition

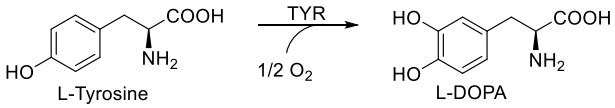

(6)

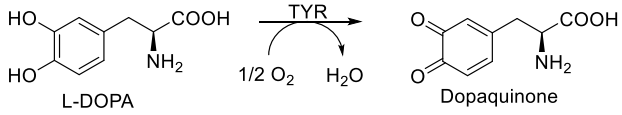

(7)

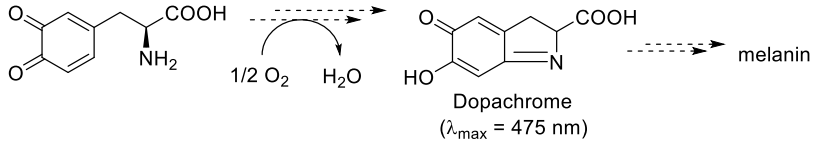

(8)

The kinetics of monophenolase and diphenolase reactions of mTYR were studied at 30°C (pH 6.8) by monitoring the oxygen consumption, respectively during the oxidation of L-tyrosine to L-Dopa (6) or of L-Dopa to dopaquinone (DQ) (7), and recording the initial rate as a function of the concentration of the substrate, to afford the typical Michaelis-Menten (M-M) hyperbolic curve (eq.1) (Guo et al., 2022). At each concentration of substrate, the reaction was performed under identical settings either in the absence of inhibitors or in the presence of different concentrations of bakuchiol, clearly showing significant inhibition already in the low micromolar range (Figure 2). Kinetic analysis was performed by non-linear fitting to M-M equation (eq. 1, Figure 2A,C) while the linearized double reciprocal Lineweaver-Burk (L-B) plot (eq. 2, Figure 2B,D) was used to identify the inhibition mode. This approach was found to offer higher accuracy than obtaining the relevant kinetic parameters (V_{max} and K_m) from the intercepts using Lineweaver-Burk plots (Guo et al., 2022; Copeland, 2000).

Concerning the inhibition mode, both for monophenolase and diphenolase reactions, regression lines in L-B plots obtained at different concentration of inhibitor crossed at (or in close proximity to) the Y axis Figure 2B,D), implying a constant value of V_{max} – the maximum rate of enzyme reaction at saturating substrate concentration – on increasing the concentration of the inhibitor, which is

indicative of a reversible competitive inhibition (Copeland, 2000). Competitive inhibition is confirmed by analysis of V_{max} and K_m values obtained by fitting M-M curves (Figure 2A, C), collected in Table 1. While V_{max} remains constant within experimental error, the M-M constant K_m – the concentration of substrate required to produce half-maximum reaction rate – increases linearly with the concentration of the inhibitors (Guo et al., 2022; Copeland, 2000). Confirmation of this behavior, typical of competitive inhibitors, is given by the secondary M-M plots of K_m *vs* [bakuchiol] (Figures S4, S5 in Appendix).

To further confirm the above findings, the reactions were also investigated in parallel by the conventional spectrophotometric approach, monitoring the formation of dopachrome at 475 nm (6-8), under otherways identical settings. Results (Figure S2, S3 in Appendix) were in excellent agreement and the corresponding V_{max} and K_m are compared to those obtained by oxygen sensing in Table 1. Average inhibition constant K_i – the dissociation constant of the enzyme-inhibitor complex – was 6.71 ± 1.23 μM for monophenolase and 1.15 ± 0.34 μM for diphenolase reactions. Such low values indicate high inhibition potency and should be compared with the higher K_i values of 10.91 μM and 9.91 μM previously measured under similar settings for reference inhibitor kojic acid (Guo et al., 2022).

3.2 IC_{50} values for mTYR inhibition by bakuchiol

Although K_i is the most reliable parameter to quantify and compare the potency of enzyme inhibitors, as it does not depend on enzyme and substrate concentrations (Copeland, 2000), it is most common in the literature to find activity quantified by the IC_{50} values: the concentration of the inhibitor affording 50% reduction of the enzyme reaction rate. Hence IC_{50} values for bakuchiol were measured by comparing the rate of reaction at fixed enzyme activity in the absence (V_0) and presence (V_I) of increasing inhibitor concentration [I], according to Langmuir equation (9) (Guo et al., 2022; Copeland, 2000).

$$\frac{V_I}{V_0} = \frac{1}{1+\frac{[I]}{IC_{50}}} \quad (9)$$

The resulting values obtained both by O_2 uptake and by spectrophotometry are given in the Appendix (Tables S1, S2) and, as expected (Copeland, 2000), they grow linearly with the concentration of substrate. While this somewhat limits their usefulness, comparison among inhibitors is possible by referring to similar settings, *e.g.* to a standard 1 mM substrate concentration.

Our values for monophenolase and diphenolase reaction, averaged between O_2 uptake and spectrophotometry, were 37.22 ± 5.18 μM and 6.76 ± 0.73, respectively (Table 1). Reference kojic acid was investigated for comparison, affording 34.02 ± 5.51 μM and 16.86 ± 3.28 μM, at 1 mM L-tyrosine and L-DOPA, respectively, in excellent agreement with previous studies by our group (Guo et al., 2022),[22] and by others (He at al., 2021).

3.3 Fluorescence quenching study

The quenching of intrinsic tryptophan fluorescence of mTYR by inhibitors is often investigated to confirm the nature of enzyme-inhibitor interaction (Yu & Fan, 2021). To this end, the fluorescence of mTYR in 50 mM phosphate buffer (pH 6.8) in the range 290-500 nm (λ_{max} 338 nm) upon excitation at 280 nm was recorded either in the absence of inhibitor (F_0) and in the presence of growing concentration of bakuchiol (Figure 2E), in the absence of substrate. On increasing the concentration of bakuchiol fluorescence intensity (F) progressively decreased, without significant shifting of the band maxima, indicating no major change in the conformation of the protein (Yu & Fan, 2021). Stern-Volmer plot (eq.10), relating the relative fluorescence intensity to the concentration of a quencher [Q], was used to analyze the quenching type, either static or dynamic.

$$F_0/F = 1 + k_q\tau_0[Q] = 1 + K_{SV}[Q] \quad (10)$$

In eq. 10 and k_q and K_{SV} are respectively the quenching rate constant and the Stern-Volmer constant, while τ_0 ($=10^{-8}$ s) is the typical lifetime of the fluorophore in the absence of the quencher (Mátyus, Szöllósi & Jenei, 2006). Figure 2F shows that the plot was linear only at low quencher concentration,

while it shows upward curvature for higher Bak levels. This behavior is often encountered in case of static quenching, *i.e.* when the protein and the quencher form a non-emitting stable complex (Mátyus et al., 2006). The K_{SV} and k_q constants determined by fitting the plot in the linear region afforded $K_{SV} = 4.32 \times 10^5\ M^{-1}$ and $k_p = 4.32 \times 10^{13}\ M^{-1}s^{-1}$. The bimolecular quenching rate constant k_p for bakuchiol is much greater than the maximum scatter collision quenching constant of dynamic quenchers with proteins, ($2.0 \times 10^{10}\ M^{-1}s^{-1}$), which indicates that the static quenching mechanism is dominating, implying the formation of a stable complex with mTYR (Yu & Fan, 2021). Dominance of the static quenching mechanism is also confirmed by fitting the data to the modified Stern-Volmer plot for static quenching (see Figure S6 in Appendix) (Yu & Fan, 2021; Mátyus et al., 2006). The apparent binding constant (K_a) and the number of binding sites (n) for complex formation between bakuchiol and mTYR were obtained by processing fluorescence data with eq. 11 (Figure 2G) (Yu & Fan, 2021). Results were $n = 1.06$ and $K_a = 1.02 \times 10^6\ M^{-1}$ indicating a single binding site and high affinity of complex formation, fully consistent with the results of enzyme inhibition.

$$\text{Log}\,[(F_0 - F)/F] = \text{Log}K_a + n\text{Log}[Q] \quad (11)$$

3.4 EPR and ReqEPR spectroscopy of bakuchiol phenoxyl radical

Reaction of the O-H group with oxidizing or chain-carrying radicals to afford the corresponding stabilized phenoxyl radical is the key process sustaining the activity of phenolic antioxidants (Valgimigli & Pratt, 2015), hence we investigated the phenoxyl radical stability to shed more light on the antioxidant mechanism of bakuchiol.

$$^{t}\text{BOO}^{t}\text{B} \xrightarrow{h\nu} 2\,^{t}\text{BO}\bullet \quad (12)$$

$$^{t}\text{BO}\bullet + \text{BakOH} \longrightarrow {}^{t}\text{BOH} + \text{BakO}\bullet \quad (13)$$

Photolysis of di-*tert*-butylperoxide in the presence of bakuchiol in the cavity of the EPR spectrometer generated alkoxyl radicals that were trapped forming bakuchiol phenoxyl radical (eqs. 12,13), which was identified by its spectrum, reported here for the first time (Figure 3A). It showed large hyperfine splitting constants (hfsc / Gauss, Table 2) due to coupling with the two *ortho* hydrogens (6.67 G) and

with the *para* -CH= (7.05 G), and lower values for coupling with the hydrogen in vinylic position (3.27 G) and with the hydrogens in *meta*-position (1.94 G) in line with structurally related radicals (Amorati et al., 2010; Brigati et al., 2002; Amorati, Ferroni, Pedulli & Valgimigli, 2003). Accordingly, the *g*-factor = 2.0041 was typical of phenoxyl radicals and indicative of C/O coupling.

Since the reactivity of phenols like bakuchiol with radicals, hence the antioxidant activity, is dictated by the bond dissociation enthalpy (BDE) of the O-H group, we measured it by the ReqEPR technique (Johansson et al., 2010; Brigati et al., 2002), which consists in photolyzing the unknown phenol (^{U}PhOH = bakuchiol) in mixture with a reference phenol (^{R}PhOH) whose BDE(OH) is known, so to establish their equilibration (eq. 14). Measurement of the corresponding equilibrium constant (eq. 15) is achieved by numerical simulation of the EPR spectrum obtained from the mixture, due to superimposition of the EPR signals of the two radicals, which affords their relative ratio (Figure 3B). This affords the ΔH of the reaction via eq. 16 under the reasonable assumption that the entropy change is negligible ($\Delta H \approx \Delta G$) (Brigati et al., 2022). Using 2,4,6-tri-*tert*-butylphenol (TBP) as the reference, the BDE(OH) of bakuchiol was determined (eq. 17) as 81.7±0.1 kcal/mol (Table 2), which well justifies its good antioxidant activity (*vide infra*). Interestingly, this value is similar to that of the weakest OH group in (structurally related) resveratrol which, although not experimentally known, can be estimated as ~ 81.4 Kcal/mol by averaging the calculated (DFT) value (80.2 Kcal/mol) and the empirical value obtained by the group additivity rule (82.6 Kcal/mol) (Amorati et al., 2003).

$$^{R}\text{PhOH} + {}^{U}\text{PhO}\bullet \rightleftarrows {}^{R}\text{PhO}\bullet + {}^{U}\text{PhOH} \quad (14)$$

$$K_{eq} = \frac{[{}^{U}PhOH]}{[{}^{R}PhOH]} \times \frac{[{}^{R}PhO\bullet]}{[{}^{U}PhO\bullet]} \quad (15)$$

$$\Delta G^\circ = \Delta H^\circ - T\Delta S^\circ = -RT\ln K_{eq} \quad (16)$$

$$\text{BDE}({}^{U}\text{PhOH}) = \text{BDE}({}^{R}\text{PhOH}) - \Delta H^\circ \quad (17)$$

3.5 Antioxidant activity of bakuchiol in solution and in micelles

The antioxidant activity of bakuchiol was investigated by monitoring oxygen consumption during the

controlled inhibited autoxidation of reference substrates, which is the golden standard in antioxidant testing (Amorati & Valgimigli, 2018; Guo et al., 2021a; Guo et al., 2021b; Baschieri et al., 2019; Amorati et al., 2016), both in homogenous organic solution and in heterogenous micellar system.

In organic solution (PhCl, 30°C) we studied the inhibited autoxidation of two well established oxidizable substrate, styrene and cumene, having largely different oxidation rates (k_p at 30°C is 41 and 0.34 $M^{-1}s^{-1}$, respectively) thereby affording complementary information (Baschieri et al., 2019). In the autoxidation of styrene initiated by AIBN, bakuchiol produced a slow-down of the oxidation, without a detectable inhibition period, which was observed instead for reference antioxidant α-tocopherol (TOH), as shown in Figure 4A. This is due to the major difference in concentration between the oxidizable substrate and the antioxidant (six orders of magnitude), which severely challenges the apparent performance of the antioxidant. Analysis of the oxygen uptake plots by eq. 5 afforded the inhibition rate constant – the rate constant for trapping alkylperoxyl radicals – k_{inh} of 2.20×10^5 $M^{-1}s^{-1}$ (Table 2), which was about one order of magnitude lower than that of TOH (k_{inh} = 3.2×10^6 $M^{-1}s^{-1}$), nature's premiere lipid soluble antioxidant. The absence of a distinct inhibition period did not produce information on the stoichiometric factor *n*, i.e. the number of peroxyl radicals trapped by one molecule of antioxidant. This however was obtained by studying the inhibited autoxidation of cumene. Owing to the lower k_p. cumene gave clear inhibition periods in the presence of micromolar bakuchiol, which were proportional to its concentration (Figure 4B), allowing to determine *n* as 1.9 ± 0.1, which is the typical value (*n* = 2) expected for a monophenolic antioxidant. The inhibition constant $k_{inh} = 1.42 \times 10^5$ $M^{-1}s^{-1}$ is in good agreement with that measured with styrene, despite the lower oxidative chain length during inhibition (Table 2).[§] The resulting averaged (styrene and cumene) value for k_{inh} of bakuchiol in PhCl solution was 1.8×10^5 $M^{-1}s^{-1}$. This value, although lower that reference TOH, is identical within experimental error to that of well-established antioxidant resveratrol (2.0×10^5 $M^{-1}s^{-1}$ at 30°C (Amorati et al., 2003)).

The antioxidant activity in heterogenous systems was investigated using the autoxidation of methyl linoleate (MeLin, 2.74 mM) in Triton™ X-100 micelles (8 mM) initiated by water soluble AAPH at

405 37°C, which is a well-validated kinetic model (Konopko & Litwinienko, 2022). Results summarized
406 in Figure 4C show that bakuchiol gave distinct inhibition of the autoxidation, whose duration was
407 proportional to its concentration. Comparison with TOH showed almost identical duration of the
408 inhibition which afforded (eq. 3) the stoichiometric factor as $n = 1.9 \pm 0.1$, in accordance with the
409 value recorded in organic solution.
410 The inhibition constant was obtained from the slope of the inhibited period by eq. 4, as $k_{inh} = (1.6 \pm$
411 $0.3) \times 10^3$ $M^{-1}s^{-1}$ (Table 2). For comparison, reference TOH under the same experimental settings
412 afforded $k_{inh} = (1.5 \pm 0.2) \times 10^4$ $M^{-1}s^{-1}$ in good agreement with literature using the same kinetic model
413 (Konopko & Litwinienko, 2022). As also found in homogenous solution, bakuchiol traps peroxyl
414 radical in micelles about one order of magnitude slower than TOH; however, it is interesting to note
415 that its antioxidant activity in micelles is almost identical to that recently reported for resveratrol (1.5
416 $\times 10^3$ $M^{-1}s^{-1}$ at 37° pH 7 (Konopko & Litwinienko, 2022)).
417
418 *3.6 Antioxidant activity of bakuchiol O-methyl derivative MeOBak*
419 Since a previous study suggested that bakuchiol antioxidant activity is due only in part to the phenolic
420 -OH group, while the terpenic chain in 4-position also contributes by trapping radicals (Adhikari et
421 al., 2003), we synthesized the protected MeOBak derivative by O-methylation of bakuchiol, and
422 tested it as an antioxidant in parallel autoxidation studies, using the oxidation of styrene in PhCl
423 solution and of MeLin in Triton™ X-100 micelles as model systems.
424 When tested under experimental settings identical to those used of native Bak, MeOBac showed no
425 inhibition of the autoxidation of styrene (Figure 4A): similarly, no protection was observed in the
426 autoxidation of MeLin in micelles, where oxygen consumption plots recorded in the presence of
427 MeOBak were hardly distinguishable from those obtained without antioxidant (Figure 4C). This
428 allowed to exclude any direct involvement of the terpene chain in the antioxidant activity of bakuchiol
429 under our experimental settings (*vide infra*).
430

4. Discussion

Kinetic studies on tyrosinase inhibition performed in parallel both by real time O_2 sensing and by spectrophotometric monitoring of dopachrome afforded superimposable results which support each-other and demonstrate major inhibition efficacy by bakuchiol, already in the low micromolar range, at variance with a previous report that indicated very modest inhibition, even at concentration of 1 mg/mL (West et al., 2021). Inhibition is competitive both for monophenolase and diphenolase reaction, with M-M related inhibition constant K_i of 6.71 ± 1.23 μM and 1.15 ± 0.34 μM, respectively, indicating higher inhibition potency for diphenolase reaction – it should be recalled that lower values indicate higher activity. K_i values measured in kinetic studies, which represent the dissociation constant of the enzyme-inhibitor complex, are fully consistent with the K_a value of 1.02×10^6 M^{-1} determined by fluorescence quenching, which represents the apparent formation constant for such complex. Interestingly, K_i values are lower than those we previously measured for reference inhibitor kojic acid (10.91 μM and 9.91 μM for monophenolase and diphenolase inhibition respectively) (Guo et al., 2022), indicating higher bioactivity of bakuchiol.

Although less robust in quantifying inhibition potency, owing to their dependence on substrate and enzyme concentration, IC_{50} values also support high anti-tyrosinase activity of bakuchiol. Values measured by O_2 sensing ranged 12-33 μM for monophenolase inhibition and 2-18 μM for diphenolase inhibition in the tested concentration range (see Appendix), while values obtained by spectrophotometry nicely matched the above (see Appendix). Taking 1 mM substrate as reference setting for comparison and using averaged results from O_2 sensing and spectrophotometry, IC_{50} values measured here for kojic acid indicate similar activity for monophenolase inhibition (34.02 μM *vs* 37.22 μM), while for diphenolase inhibition bakuchiol (IC_{50} = 6.76 μM) was sensibly more effective than kojic acid (IC_{50} = 16.86 μM). This is at variance with a previous study reporting IC_{50} values of bakuchiol 18-folds higher than kojic acid for diphenolase inhibition (Cheng & Chen, 2017), and proves a sensibly higher anti-tyrosinase activity of bakuchiol than previously expected.

456 It was recently shown by Kang et al. (2020). that a phytoestract of *P. corylifolia* containing 77%
457 bakuchiol reduced melanin biosynthesis in normal human epidermal melanocytes and the activity
458 was attributed to reduction of tyrosinase enzyme expression and to reduction of TRP-1, TRP-2 and
459 SOX-9 supporting proteins in melanocytes, without significant toxicity. The study showed also a
460 downregulation of melanocyte dendrites formation, necessary to the transfer of melanosomes to
461 neighboring keratinocytes. Our current data highlight an additional complementary mechanism for
462 the depigmenting activity outlined in that (Kang et al., 2020) and other studies (Dhaliwal et al., 2019;
463 West et al., 2021): the potent inhibition of tyrosinase reaction. This hopefully completes the picture
464 allowing full rationalization of bakuchiol's depigmenting activity. Most important, it opens to new
465 applications of bakuchiol based on its interference with tyrosinase chemistry (*vide infra*).
466 Being a phenolic compound, the antioxidant activity of bakuchiol is expectedly dictated by its ability
467 to quench chain-carrying peroxyl radicals to the corresponding hydroperoxide, by formal H-atom
468 transfer from the phenolic OH (18) (Amorati & Valgimigli, 2018). Inhibited autoxidation studies
469 indicated a stoichiometric factor $n \sim 2$ (1.9±0.1) both in organic solution and in aqueous micelles;
470 therefore, a second peroxyl radical is trapped by the resulting phenoxyl radical, most typically by
471 addition to the aromatic ring in conjugated positions (arrows in eq. 19) (Valgimigli & Pratt, 2015),
472 or possibly by styryl-type addition (19).

473 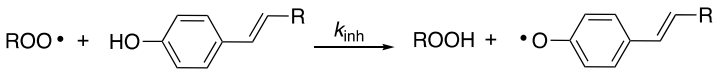

(18)

474 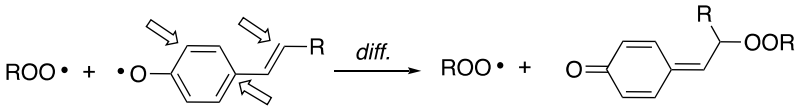

(19)

475 Wherever the second ROO• trapping occurs, it is not regulating the antioxidant activity, which is
476 dictated by rate-determining reaction 18 (Amorati & Valgimigli, 2018). Since the BDE(OH) of the
477 alkylhydroperoxides is 88.6 kcal/mol (Amorati et al., 2011; Amorati, Menichetti, Mileo, Pedulli &
478 Viglianisi, 2009), our present measurement of the BDE(OH) of bakuchiol by ReqEPR as 81.7

kcal/mol affords the $\Delta H°$ of reaction 18 as -6.9 kcal/mol, which justifies bakuchiol's efficient trapping of ROO• radicals (k_{inh} = 1.8 × 10^5 $M^{-1}s^{-1}$ in PhCl solution at 30°C).

Indeed, the BDE(OH) value of bakuchiol can be correlated to its reactivity via linear Evans-Polanyi relationships between log(k_{inh}) and BDE(OH), which are well established for phenolic antioxidants Amorati, et al., 2009). When such a plot is built for differently substituted phenols using literature data in apolar organic solution (Johansson et al., 2010; Amorati, et al., 2009), parallel correlations lines are observed depending on the steric hindrance in *ortho*-position to the reactive OH group (Figure 4D). It should be noted that bakuchiol perfectly fits in the correlation line for phenols lacking *ortho* substituents, implying that its reactivity with peroxyl radicals stems entirely from reaction of the phenolic OH group, while the terpenoid chain would influence its reactivity only due to its electronic properties, *i.e.* by stabilizing the phenoxyl radical and lowering the BDE(OH).

Our findings are at variance with a previous study which attributed part of the antioxidant activity of bakuchiol to the terpenoid chain (Adhikari, et al., 2003). This conclusion was drawn mainly for the finding that the O-methylated derivative (MeOBak) reacted with thiyl radicals (by H-abstraction in the allyl positions) forming detectable transient species. However, it should be noted that the reaction of the side chain with some radical does not imply its antioxidant action. Indeed, the formed C-centered radical (R•) would rapidly react with oxygen forming an alkylperoxyl radical ROO• that likely propagates the oxidative chain (Amorati & Valgimigli, 2018). As a proof of concept, we prepared MeOBak and tested it as an antioxidant both in the autoxidation of styrene in solution and of MeLin in micelles. Our results indicated no antioxidant activity of MeOBak in both systems under our testing conditions, confirming that the antioxidant activity of bakuchiol stems entirely from the phenolic OH, while the side chain would contribute by increasing its reactivity. However, it is possible that at much higher concentration and depending on the exact experimental settings, the terpenic chain would have chain termination-enhancing behavior, and show some minor antioxidant activity via a different mechanism we previously disclosed for non-phenolic terpenoids like linalool (Baschieri, Ajvazi, Tonfack, Valgimigli, & Amorati, 2017).

The lower antioxidant activity of bakuchiol in micelles compared to apolar organic solution (k_{inh} of 1.6×10^3 $M^{-1}s^{-1}$ *vs* 1.8×10^5 $M^{-1}s^{-1}$) follows the well-known behavior of any phenolic antioxidant and it pairs with a similar reduction in activity of reference TOH (k_{inh} from 3.2×10^6 $M^{-1}s^{-1}$ to 1.5×10^4 $M^{-1}s^{-1}$). It is partly due to H-bonding of the phenolic OH group at the water-lipid interface and partly due to rate-limiting exchange of radicals and antioxidants among micellar particles (Amorati et al., 2016).

It is interesting to note that, both in apolar organic solution and in aqueous micelles, the antioxidant activity of bakuchiol perfectly matches that of well-established antioxidant resveratrol, which boosts the interest for the potential applications of bakuchiol.

The co-existence of good antioxidant activity and high tyrosinase inhibiting activity fully justifies the interest for bakuchiol in topical skin-care treatments, *e.g.* against photoaging (Chaudhuri et al., 2014; Dhaliwal et al., 2019; West et al. 2021; Mahdavi et al., 2022; Zhu et al., 2022), which meets a growing demand for plant-derived compounds with such bioactivity (Panzella & Napolitano, 2019).

Most interestingly, our results also suggest a previously overlooked potential of bakuchiol: its use as natural food preservative. Not only bakuchiol outperforms reference kojic acid as tyrosinase inhibitor, it also outperforms by over one order of magnitude the efficacy in peroxyl radical trapping of ubiquitous food preservative butylated hydroxytoluene (BHT, $k_{inh} \sim 1 \times 10^4$ $M^{-1}s^{-1}$ at 30°C in PhCl) (Amorati et al., 2003), promising much improved protection against oxidative damage combined with excellent protection from enzymatic food-browning.

5. Conclusions

This study addresses for the first time on quantitative grounds the kinetics of tyrosinase inhibition and of peroxyl radical trapping by bakuchiol, highlighting anti-tyrosinase activity significantly higher than previously expected, with competitive mechanism both toward monophenolase and diphenolase reactions and K_i values of 6.71±1.23 µM and 1.15±0.34 µM respectively. These values are significantly lower than the values for reference kojic acid implying higher potency, confirmed also

by the measured IC_{50} values (1 mM substrate) of 37.22 μM, and 6.76 μM for monophenolase and diphenolase inhibition by bakuchiol *vs* 34.02 μM and 16.86 μM for kojic acid. This verifies our initial hypothesis. At the same time, the rate constant of peroxyl radical trapping k_{inh} of 1.8×10^5 $M^{-1}s^{-1}$ (PhCl solution) and the corresponding value in aqueous micelles are indistinguishable from those of well-established antioxidant resveratrol (Konopko & Litwinienko, 2022) and over 10-folds larger than those of ubiquitous food preservative BHT (Amorati et al., 2003). They stem entirely from the phenolic function and justify the interest for this food-borne molecule. While our quantitative data help rationalize the activity shown in skin-care treatments (Dhaliwal et al., 2019; West et al. 2021;), the combination of such two properties (anti-tyrosinase and antioxidant) offers full rational for a previously overlooked application as natural food preservative, potentially able to contrast food spoilage arising both from air oxidation and from enzymatic browning, which are regarded in the food industry as the main undesired events in post-harvest processing and preservation of fresh food (Mahdavi et al., 2022). The lack of significant toxicity arising from previous studies (Dhaliwal et al., 2019; Kang et al., 2020) and the reported antimicrobial/antifungal activities (Alam et al., 2018) make this phytochemical even more interesting in this regard. Thus, our current results call for further research to fully explore the previously overlooked potential of bakuchiol in the food industry.

Abbreviations

AAPH, 2,2'-azobis(2-amidinopropane) dihydrochloride; AIBN, 2,2′-azobis(isobutyronitrile); Bak, bakuchiol; L-DOPA, levo-dihydroxyphenylalanine; MeLin, methyl linoleate; mTYR, mushroom tyrosinase; OSS, oxidative stress status; ROS, reactive oxygen species; SOX9, 9th transcription factor of the Sry high-mobility-group-box family; TBP, 2,4,6-tri-*tert*-butylphenol; α-TOH, alpha-tocopherol; TRP-1, tyrosinase related protein 1; TRP-2, tyrosinase related protein 2; TYR, tyrosinase.

Declaration of interest

The authors declare no competing financial interest.

Acknowledgments

We thank Marco Lucarini for access to EPR simulation software and Riccardo Amorati for helpful discussion.

Funding Sources

This work was supported by the University of Bologna (Grant: RFO2021).

Appendix A. Supplementary data

GC-MS analysis of bakuchiol and MeOBak, kinetic plots of tyrosinase inhibition monitored by spectrophotometry, tables of IC_{50} values of bakuchiol, additional plots of fluorescence quenching and additional ReqEPR spectra, oxygen uptake during anzymatic vs. spontaneous oxidation of Dopa.

Notes

[†] DOPA in aqueous solution undergoes spontaneous autocatalytic oxidation (Roginsky, Barsukova, Bruchelt, & Stegmann, 1997); however, this was estimated to account for less than 2% of our measured rates of mTYR-catalyzed reaction, having non-significant influence on the reported kinetics (see Appendix, Figure S8).

[§] In cumene TOH produced complete inhibition (not shown) *i.e.* the chain length ν_{inh} was close to 1, therefore it was used as a reference only for measuring the rate of initiation R_i via eq 3.

References

Adhikari, S., Joshi, R., Patro, B. S., Ghanty, T.K., Chintalwar, G.J., Sharma, A., Chattopadhyay, S. & Mukherjee, T. (2003) Antioxidant Activity of Bakuchiol: Experimental Evidences and Theoretical Treatments on the Possible Involvement of the Terpenoid Chain. *Chem. Res. Toxicol. 16*, 1062-1069. DOI: 10.1021/tx034082r.

Alam, F., Khan, G. N. & Asad, M. H. H. B. (2018) Psoralea corylifolia L: Ethnobotanical, biological, and chemical aspects: A review. *Phytother. Res. 32*, 597–615. DOI: 10.1002/ptr.6006

582 Amorati, R., Pedulli, G. F. & Valgimigli, L. (2011) Kinetic and thermodynamic aspects of the chain-
583 breaking antioxidant activity of ascorbic acid derivatives in non-aqueous media. *Org. Biomol.*
584 *Chem. 9*, 3792-3800. DOI: 10.1039/c1ob05334e.
585 Amorati, R. & Valgimigli, L. (2018) Methods To Measure the Antioxidant Activity of
586 Phytochemicals and Plant Extracts. *J. Agric. Food Chem. 66*, 3324−3329. DOI:
587 10.1021/acs.jafc.8b01079.
588 Amorati, R., Baschieri, A., Morroni, G., Gambino, R. & Valgimigli, L. (2016) Peroxyl Radical
589 Reactions in Water Solution: A Gym for Proton-Coupled Electron-Transfer Theories. *Chem.*
590 *Eur. J. 22*, 7924 - 7934. DOI: 10.1002/chem.201504492.
591 Amorati, R., Ferroni, F., Pedulli, G. F. & Valgimigli, L. (2003) Modeling the Co-Antioxidant
592 Behavior of Monofunctional Phenols. Applications to Some Relevant Compounds. *J. Org.*
593 *Chem. 68*, 9654-9658. DOI: 10.1021/jo0351825.
594 Amorati, R., Menichetti, S., Mileo, E., Pedulli, G. F. & Viglianisi, C. (2009) Hydrogen-Atom
595 Transfer Reactions from ortho-Alkoxy-Substituted Phenols: An Experimental Approach.
596 *Chem. Eur. J. 15*, 4402–4410. DOI: 10.1002/chem.200802454.
597 Amorati, R., Pedulli, G. F., Valgimigli, L., Johansson, H. & Engman, L. (2010) Organochalcogen
598 substituents in phenolic antioxidants. *Org. Lett. 12*, 2326 – 2329. DOI: 10.1021/ol100683u.
599 Baschieri, A., Ajvazi, M. D., Tonfack, J. L. F., Valgimigli, L. & Amorati, R. (2017) Explaining the
600 antioxidant activity of some common non-phenolic components of essential oils. *Food Chem.*
601 *232*, 656–663. DOI: 10.1016/j.foodchem.2017.04.036.
602 Baschieri, A., Pizzol, R., Guo, Y., Amorati, R. & Valgimigli, L. (2019) Calibration of Squalene,
603 p-Cymene, and Sunflower Oil as Standard Oxidizable Substrates for Quantitative Antioxidant
604 Testing. *J. Agric. Food Chem. 67*, 6902−6910. DOI: 10.1021/acs.jafc.9b01400.
605 Brigati, G., Lucarini, M., Mugnaini, V. & Pedulli, G.F. (2002) Determination of the Substituent Effect
606 on the O-H Bond Dissociation Enthalpies of Phenolic Antioxidants by the EPR Radical
607 Equilibration Technique. *J. Org. Chem. 67*, 4828-4832. DOI: 10.1021/jo025755y.

608 Chaudhuri, R. K. & Bojanowski, K. (2014) Bakuchiol: a retinol-like functional compound revealed
609 by gene expression profiling and clinically proven to have anti-aging effects. *International*
610 *Journal of Cosmetic Science*, *36*, 221–230. DOI: 10.1111/ics.12117
611 Cheng, M. & Chen, Z. (2017) Screening of tyrosinase inhibitors by capillary electrophoresis with
612 immobilized enzyme microreactor and molecular docking. *Electrophoresis*, *38*, 486–493.
613 DOI 10.1002/elps.201600367.
614 Chopra, B., Dhingra, A. K. & Dhar, K. L. (2013) Psoralea corylifolia L. (Buguchi) — Folklore to
615 modern evidence: Review. *Fitoterapia*, *90*, 44–56. DOI: 10.1016/j.fitote.2013.06.016
616 Copeland, R. A. (2000) Enzymes: A Practical Introduction to Structure, Mechanism, and Data
617 Analysis (2nd Ed.). Wiley-VCH, New York. ISBN: 0-471-22063-9.
618 Dhaliwal, S., Rybak, I., Ellis, S. R., Notay, M., Trivedi, M., Burney, W., Vaughn, A. R., Nguyen, M.,
619 Reiter, P., Bosanac, S., Yan, H., Foolad, N. & Sivamani, R. K. (2019) Prospective,
620 randomized, double-blind assessment of topical bakuchiol and retinol for facial photoageing.
621 *Brit. J. Dermatol. 180*, 289–296. DOI 10.1111/bjd.16918.
622 Fenoll, L. G., Rodriguez-Lopez, J. N., Garcia-Molina, F., Garcìa-Canovas, F. & Tudela, J. (2002)
623 Unification for the Expression of the Monophenolase and Diphenolase Activities of
624 Tyrosinase. *IUBMB Life*, *54*, 137–141. DOI:10.1080/15216540214537
625 Guo, Y., Baschieri, A., Amorati, R. & Valgimigli, L. (2021a) Synergic antioxidant activity of γ-
626 terpinene with phenols and polyphenols enabled by hydroperoxyl radicals. *Food Chem.*, *345*,
627 128468. DOI: 10.1016/j.foodchem.2020.128468.
628 Guo, Y., Baschieri, A., Mollica, F., Valgimigli, L., Cedrowski, J., Litwinienko, G. & Amorati, R.
629 (2021b) Hydrogen Atom Transfer from HOO to ortho-Quinones Explains the Antioxidant
630 Activity of Polydopamine. *Angew. Chem. Int. Ed.*, *60*, 15220–15224. DOI:
631 10.1002/anie.202101033.

Guo, Y., Cariola, A., Matera, R., Gabbanini, S. & Valgimigli, L. (2022) Real-time oxygen sensing as a powerful tool to investigate tyrosinase kinetics allows revising mechanism and activity of inhibition by glabridin. *Food Chem. 393*, 133423 DOI: 10.1016/j.foodchem.2022.133423

Haraguchi, H., Inoue, J., Tamura, Y. & Mizutani, K. (2000) Inhibition of Mitochondrial Lipid Peroxidation by Bakuchiol, a Meroterpene from Psoralea corylifolia. *Planta Med. 66*, 569-571. DOI: 10.1055/s-2000-8605.

He, M., Fan, M., Liu, W., Li, Y. & Wang, G. (2021) Design, synthesis, molecular modeling, and biological evaluation of novel kojic acid derivatives containing bioactive heterocycle moiety as inhibitors of tyrosinase and antibrowning agents. *Food Chemistry, 362*, 130241. DOI: 10.1016/j.foodchem.2021.130241

Hu, G. & Brenner-Moyer, S. E. (2022) Combining Palladium and Chiral Organocatalysis for the Enantioselective Deconjugative Allylation of Enals via Dienamine Intermediates. *J. Org. Chem. 87*, 866−873. DOI: 10.1021/acs.joc.1c02591

Johansson, H., Shanks, D., Engman, L., Amorati, R., Pedulli, G. F. & Valgimigli, L. (2010) Long-lasting antioxidant protection: A regenerable BHA analogue. *J. Org. Chem. 75*, 7535 - 754119. DOI: 10.1021/jo101239c.

Kang, M. C., Lee, J.-W., Lee, T. H., Subedi, L., Wahedi, H. M., Do, S.-G., Shin, E., Moon, E.-Y. & Kim, S. Y. (2020) UP256 Inhibits Hyperpigmentation by Tyrosinase Expression/Dendrite Formation via Rho-Dependent Signaling and by Primary Cilium Formation in Melanocytes. *Int. J. Mol. Sci. 21*, 5341. DOI: 10.3390/ijms21155341

Konopko, A. & Litwinienko, G. (2022) Unexpected Role of pH and Microenvironment on the Antioxidant and Synergistic Activity of Resveratrol in Model Micellar and Liposomal Systems. *J. Org. Chem. 87*, 1698−1709. DOI: 10.1021/acs.joc.1c01801.

Krishna, A. T. P., Edachery, B. & Athalathil, S. (2022) Bakuchiol – a natural meroterpenoid: structure, isolation, synthesis and functionalization approaches. *RSC Adv. 12*, 8815–8832. DOI: 10.1039/d1ra08771a.

Mahdavi, A., Mohammadsadeghi, N., Mohammadi, F., Saadati, F. & Nikfard. S. (2022) Evaluation of inhibitory effects of some novel phenolic derivatives on the mushroom tyrosinase activity: Insights from spectroscopic analyses, molecular docking and in vitro assays. *Food Chemistry, 387,* 132938. DOI: 10.1016/j.foodchem.2022.132938

Mátyus, L. Szöllósi, J. & Jenei, A. (2006) Steady-state fluorescence quenching applications for studying protein structure and dynamics. *J. Photochem. Photobiol. B, 83,* 223–236. DOI: 10.1016/j.jphotobiol.2005.12.017.

McGrath, A. J., Garrett, G. E., Valgimigli, L. & Pratt, D. A. (2010) The redox chemistry of sulfenic acids. *J. Am. Chem. Soc. 132*, 16759 – 167611. DOI: 10.1021/ja1083046.

Oh, K. Y., Lee, J. H., Curtis-Long, M. J., Cho, J. K., Kim, J. Y., Lee, W. S. & Park, K. H. (2010) Glycosidase inhibitory phenolic compounds from the seed of Psoralea corylifolia. *Food Chemistry, 121,* 2010, 940-945. DOI: 10.1016/j.foodchem.2010.01.022

Panzella, L. & Napolitano, A. (2019) Natural and Bioinspired Phenolic Compounds as Tyrosinase Inhibitors for the Treatment of Skin Hyperpigmentation: Recent Advances. *Cosmetics, 6,* 57. DOI: 10.3390/cosmetics6040057.

Roginsky, V. A., Barsukova, T. K., Bruchelt, G. & Stegmann, H. B. (1997) The Oxidation of Catecholamines and 6-Hydroxydopamine by Molecular Oxygen: Effect of Ascorbate. *Z. Naturforsch., 52c,* 380-390. DOI: 10.1515/znc-1997-5-617.

Song, X., Ni, M., Zhang, Y., Zhang, G., Pan, J. & Gong, D. (2021) Comparing the inhibitory abilities of epigallocatechin-3-gallate and gallocatechin gallate against tyrosinase and their combined effects with kojic acid. *Food Chemistry, 349,* 129172. DOI: 10.1016/j.foodchem.2021.129172

Valgimigli, L. & Pratt, D. A. (2015) Maximizing the reactivity of phenolic and aminic radical-trapping antioxidants: Just add nitrogen! *Acc. Chem. Res. 48,* 966 – 97521. DOI: 10.1021/acs.accounts.5b00035.

683 Valgimigli, L., Valgimigli, M., Gaiani, S., Pedulli, G. F. & Bolondi, L. (2000) Measurement of
684 oxidative stress in human liver by EPR spin-probe technique. *Free Radic. Res. 33*, 167 – 178.
685 DOI: 10.1080/10715760000300721.
686 West, B. J., Alabi, I. & Deng, S. (2021) A Face Serum Containing Palmitoyl Tripeptide-38,
687 Hydrolyzed Hyaluronic Acid, Bakuchiol and a Polyherbal and Vitamin Blend Improves Skin
688 Quality. *J. Cosm., Dermatol. Sci. App., 11*, 237-252. DOI: 10.4236/jcdsa.2021.113020.
689 Yang, D., Wang, L., Zhai, J., Han, N., Liu, Z., Li, S. & Yin, J. (2021) Characterization of
690 antioxidant, α-glucosidase and tyrosinase inhibitors from the rhizomes of Potentilla anserina
691 L. and their structure–activity relationship. *Food Chemistry, 336,* 127714. DOI:
692 10.1016/j.foodchem.2020.127714.
693 Yu, Q. & Fan, L. (2021) Understanding the combined effect and inhibition mechanism of 4-
694 hydroxycinnamic acid and ferulic acid as tyrosinase inhibitors. *Food Chem., 352,* Article
695 129369. DOI: 10.1016/j.foodchem.2021.129369.
696 Zhu, Y.-Z., Chen, K., Chen, Y.-L., Zhang, C., Xie, Y.-Y., Hider, R. C. & Zhou, T. (2022) Design
697 and synthesis of novel stilbene-hydroxypyridinone hybrids as tyrosinase inhibitors and their
698 application in the anti-browning of freshly-cut apples. *Food Chemistry, 385*, 132730. DOI:
699 10.1016/j.foodchem.2022.132730.
700

Table 1. Kinetic parameters of tyrosinase inhibition by bakuchiol at 30°C (pH = 6.8). Kinetic data were obtained by non-linear fitting of M-M plots at different bakuchiol concentrations, by O_2 sensing and UV-Vis spectrophotometry.[a]

Monophenolase (substrate = L-tyrosine)					
O_2 Uptake					
Bakuchiol (**μ*M***)	K_m or K_m^{app} (mM)	V_m or V_m^{app} (μM/min)	K_I (μM)	Average K_I (μM)	IC_{50} (μM) 1 mM substr.
0	0.19 ± 0.02	4.20 ± 0.10	-	6.93 ±0.93	33.35 ±3.41
1	0.21 ± 0.01	3.98 ± 0.25	8.04		
2	0.26 ± 0.03	3.96± 0.05	5.80		
4	0.30 ± 0.02	4.02 ± 0.10	7.11		
8	0.41 ± 0.04	4.00 ± 0.17	6.76		
UV-Vis Spectrophotometry (dopachrome formation)					
Bakuchiol (**μ*M***)	K_m or K_m^{app} (mM)	V_m or V_m^{app} (μM/min)	K_I (μM)	Average K_I (μM)	IC_{50} (μM) 1 mM substr.
0	0.19 ± 0.02	4.11 ± 0.14	-	6.49 ±0.58	41.09 ±3.12
1	0.22 ± 0.02	4.13 ± 0.16	5.92		
4	0.30 ± 0.01	4.12 ± 0.07	6.48		
8	0.40 ± 0.03	4.16 ± 0.13	7.07		
Averaged values (O_2 and UV-Vis)				6.71 ± 1.23	37.22 ± 5.18

Diphenolase (substrate = L-DOPA)					
O_2 Uptake					
Bakuchiol (**μM**)	K_m or K_m^{app} (mM)	V_m or V_m^{app} (μM/min)	K_I (μM)	Average K_I (μM)	IC_{50} (μM) 1 mM substr.
0	0.20 ± 0.01	9.84 ± 0.07	-	1.16 ±0.28	7.06 ±0.42
0.5	0.32 ± 0.02	9.73 ± 0.17	0.81		
1	0.38 ± 0.02	9.62 ± 0.16	1.07		
2	0.49 ± 0.03	9.75 ± 0.20	1.33		
4	0.75 ± 0.09	9.82 ± 0.42	1.44		
UV-Vis Spectrophotometry (dopachrome formation)					
Bakuchiol (**μM**)	K_m or K_m^{app} (mM)	V_m or V_m^{app} (μM/min)	K_I (μM)	Average K_I (μM)	IC_{50} (μM) 1 mM substr.
0	0.20 ± 0.02	10.26 ± 0.25	-	1.13 ±0.12	6.76 ±0.73
0.5	0.30 ± 0.03	9.98 ± 0.24	1.03		
1	0.36 ± 0.05	10.12 ± 0.38	1.26		
2	0.56 ± 0.09	9.73 ± 0.51	1.11		
Averaged values (O_2 and UV-Vis)				1.15 ± 0.34	6.91 ± 0.96

[a] V_{max} and K_m or V_{max}^{app} and K_m^{app} refer to not inhibited and inhibited assays, respectively. †

Table 2. EPR spectral parameters of bakuchiol phenoxyl radical, BDE(OH) determined by ReqEPR radical equilibration at 30°C in *tert*-butyl-benzene (n = 10), rate constants for trapping peroxyl radicals (k_{inh}) and stoichiometric factor (n) measured in the autoxidation of styrene and cumene in homogenous solution (PhCl, 30°C), and of MeLin dispersed in Triton X-100 micelles (37°C), all inhibited by bakuchiol.

Thermodynamics of the -OH group			
Radical	hfsc / Gauss [a]		*g*-factor
Bak(•)	6.67 ($2H_{ortho}$); 1.94 ($2H_{meta}$); 7.05 (H_{para}); 3.27 (H_{vinyl})		2.0041
TBP(•)	1.77 ($2H_{meta}$); 0.18 (18H)		2.0046
^{U}PhOH	^{R}PhOH	K_{eq}	BDE (Kcal/mol)
Bak	TBP	14.25 ± 2.07	81.7 ± 0.1
Kinetics of ROO• trapping			
Substrate (medium)	k_{inh} (10^4 $M^{-1}s^{-1}$)	n [b]	ν_{inh} [c]
Styrene (solution)	22.0 ± 3.0	n.d.	172
Cumene (solution)	14.2 ± 2.2	1.9 ± 0.1	7.5
Average in solution	18.1 ± 6.6	1.9 ± 0.1	
MeLin (micelles)	0.16 ± 0.03	1.9 ± 0.1	10.6

[a] Hyperfine splitting constants in Gauss (= 0.1 Tesla). [b] Stoichiometric factor = number of peroxyl radical trapped by one molecule of antioxidant. [c] Kinetic chain length $\nu_{inh} = R_{inh}/R$

FIGURE CAPTIONS

Figure 1. Structure of investigated bakuchiol and the methyl ether compared to retinol.

Figure 2. (A-C) Kinetics of mTYR reaction (30°C, pH 6.8) monitored by O_2 uptake, inhibited by bakuchiol, for (A, B) monophenolase reaction (substrate = L-Tyrosine; mTYR 1.6 U/mL) and (C, D) diphenolase reaction (substrate = L-DOPA, mTYR 0.8 U/mL). Graphs represent Michaelis-Menten hyperbolic plots (A, C) and Lineweaver-Burk linear plots (B, D) of the same experiments. (E-G) Fluorescence emission spectra of mTYR (20 U/mL) in the absence (a) and the presence (b-k) of increasing concentration of bakuchiol up to 1.320 µM (E), the corresponding Stern-Volmer plot (F), and the log-log plot (eq. 11) relating fluorescence quenching to the number of binding sites (*n*) and complex formation constant K_a (G).

Figure 3. EPR (X-band) spectrum recorded by photolyzing in the cavity of the spectrometer (in *tert*-butylbenzene/^{t}BOO^{t}B 9:1, at 30°C): (A) bakuchiol, (B) a mixture of bakuchiol and TBP 20:1. Simulations were obtained by Monte Carlo method using the parameters in Table 2. The spectral lines due to TBP• radical are indicated by an arrow (B): the resulting radical ratio was 1.26:1 (Bak•/TBP•).

Figure 4. Oxygen consumption plots recorded during the autoxidation of 4.3 M styrene in PhCl (A), and 3.6 M cumene in PhCl (B), both initiated by AIBN (0.05 M) at 30°C, or of 2.74 mM MeLin in 8 mM Triton™ X-100 micelles initiated by 5 mM AAPH at 37°C, pH 7 (C), without inhibitors (dashed line) or in the presence of bakuchiol, or MeOBak, or TOH, as indicated. Thin lines represent the regression of the inhibited periods. In panel (D) Evans-Polanyi correlation of the rate constant k_{inh} (at 30°C) for trapping ROO• radicals by phenols with 2,6 (*ortho*) substituents of different size *vs* their BDE(OH). The data point of bakuchiol is indicated by a full star (★).

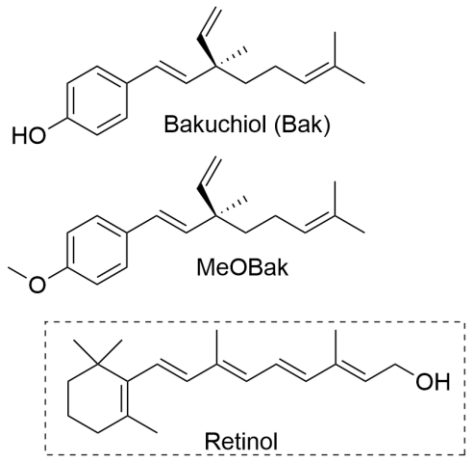

Figure 1. Structures of investigated bakuchiol and the methyl ether compared to retinol.

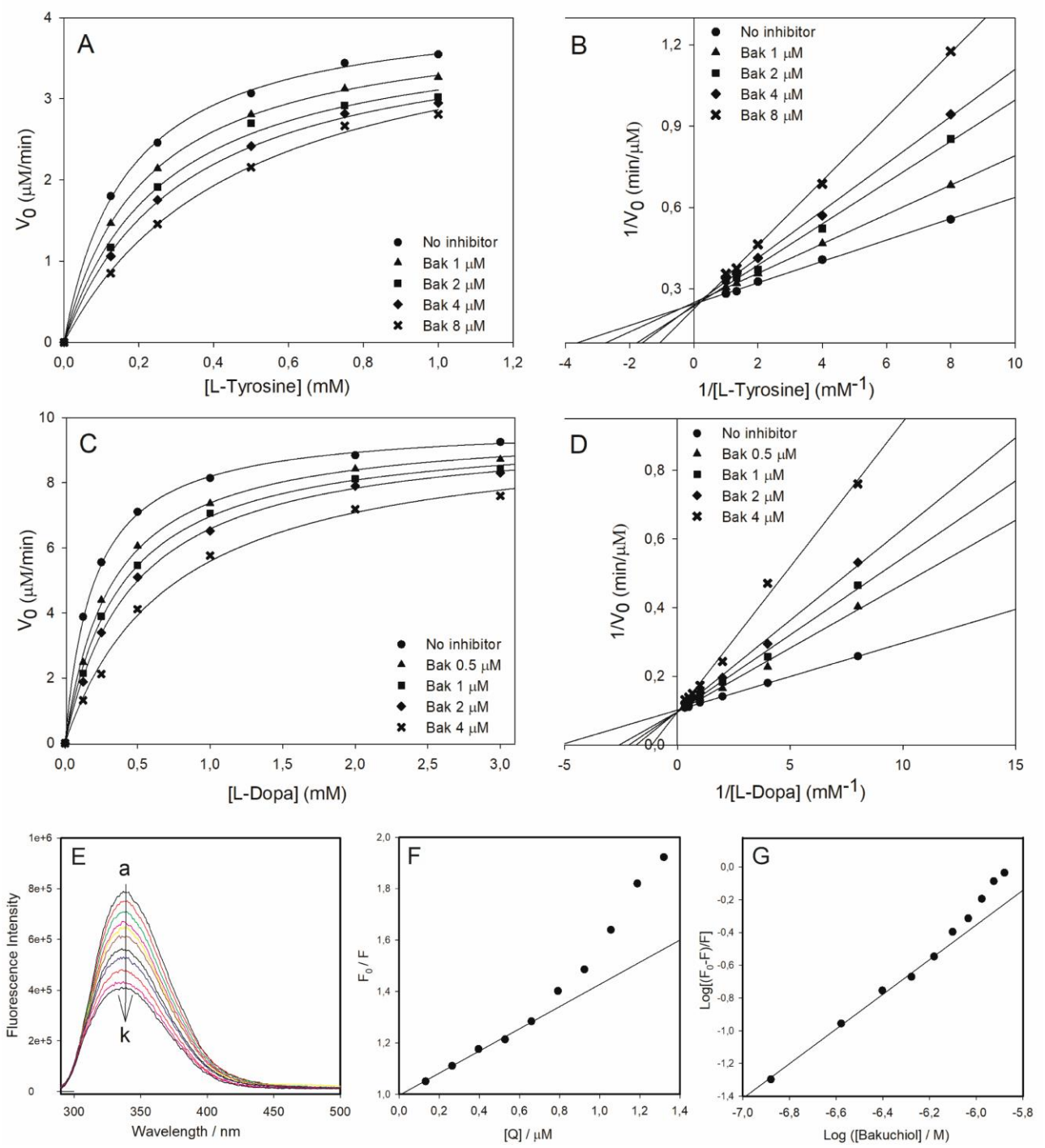

Figure 2. (A-C) Kinetics of mTYR reaction (30°C, pH 6.8) monitored by O_2 uptake, inhibited by bakuchiol, for (A, B) monophenolase reaction (substrate = L-Tyrosine; mTYR 1.6 U/mL) and (C, D) diphenolase reaction (substrate = L-DOPA, mTYR 0.8 U/mL). Graphs represent Michaelis-Menten hyperbolic plots (A, C) and Lineweaver-Burk linear plots (B, D) of the same experiments. (E-G) Fluorescence emission spectra of mTYR (20 U/mL) in the absence (a) and the presence (b-k) of increasing concentration of bakuchiol up to 1.320 μM (E), the corresponding Stern-Volmer plot (F), and the log-log plot (eq. 11) relating fluorescence quenching to the number of binding sites (*n*) and complex formation constant K_a (G).

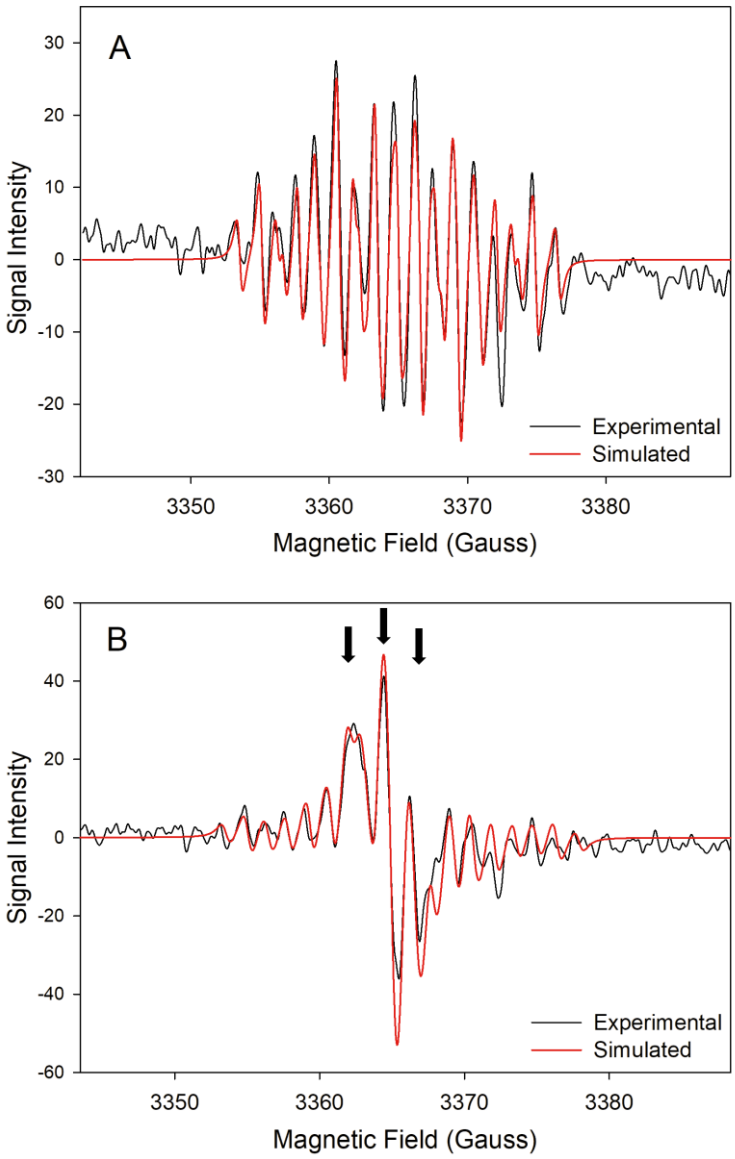

Figure 3. EPR (X-band) spectrum recorded by photolyzing in the cavity of the spectrometer (in *tert*-butylbenzene/^{t}BOO^{t}B 9:1, at 30°C): (A) bakuchiol, (B) a mixture of bakuchiol and TBP 20:1. Simulations were obtained by Monte Carlo method using the parameters in Table 2. The spectral lines due to TBP• radical are indicated by an arrow (B): the resulting radical ratio was 1.26:1 (Bak•/TBP•).

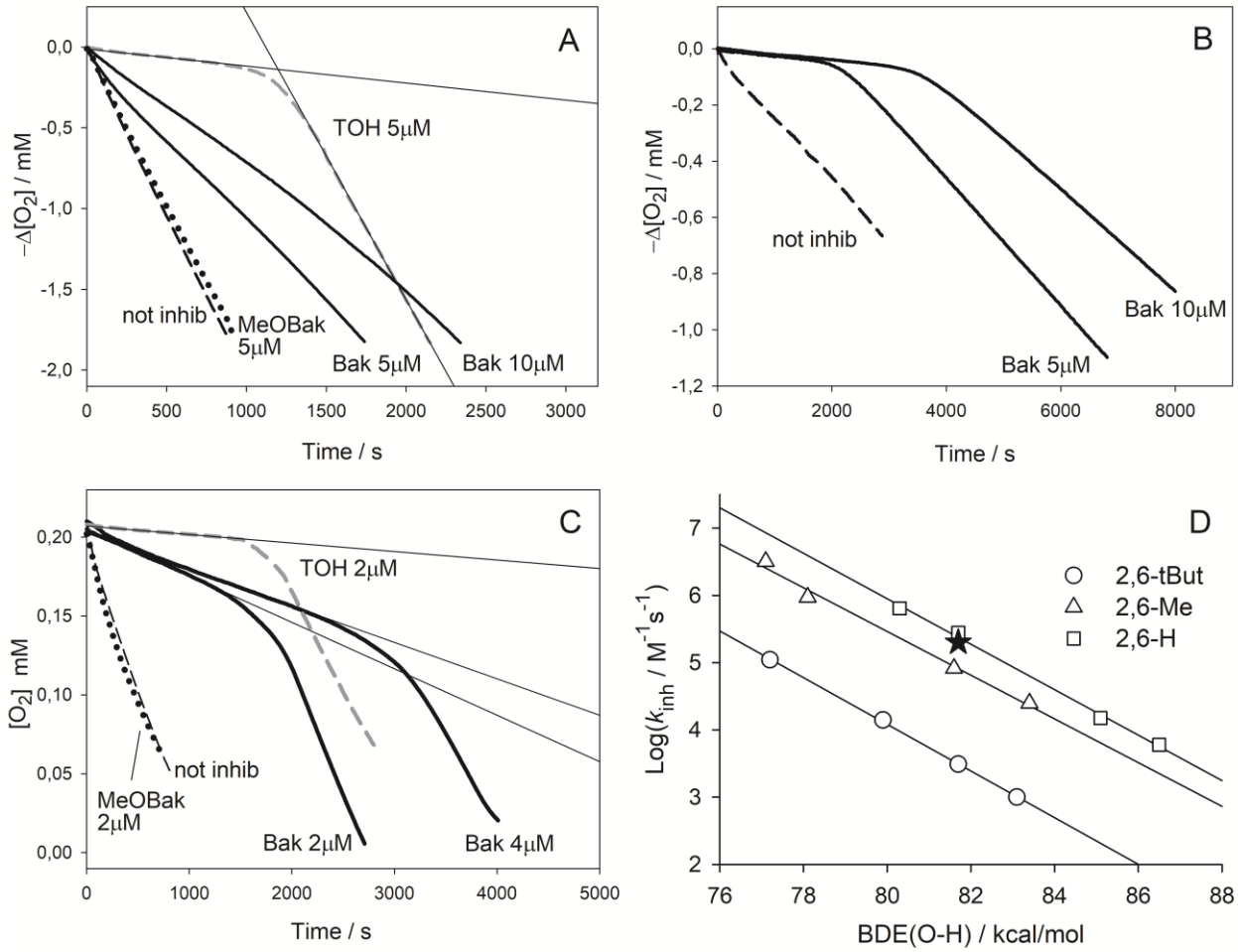

Figure 4. Oxygen consumption plots recorded during the autoxidation of 4.3 M styrene in PhCl (A), and 3.6 M cumene in PhCl (B), both initiated by AIBN (0.05 M) at 30°C, or of 2.74 mM MeLin in 8 mM Triton X-100 micelles initiated by 5 mM AAPH at 37°C, pH 7 (C), without inhibitors (dashed line) or in the presence of bakuchiol, or MeOBak, or TOH as indicated. Thin lines represent the regression of the inhibited periods. In panel (D) Evans-Polanyi correlation of the rate constant k_{inh} (at 30°C) for trapping ROO• radicals by phenols with 2,6 (*ortho*) substituents of different size *vs* their BDE(OH). The data point of bakuchiol is indicated by a full star (★).

Graphical abstract